Tropism of SARS-CoV-2 in commonly used laboratory cell lines and their proteomic landscape during infection

Elisa Saccon[1&], Xi Chen[1&], Flora Mikaeloff[1&], Jimmy Esneider Rodriguez[2], Laszlo Szekely[3], Beatriz Sá Vinhas[1], Shuba Krishnan[1], Siddappa N. Byrareddy[4], Teresa Frisan[6], Ákos Végvári [2], Ali Mirazimi[1,5], Ujjwal Neogi[1], Soham Gupta[1*]

[1]Division of Clinical Microbiology, Department of Laboratory Medicine, Karolinska Institutet, Stockholm, Sweden.
[2]Division of Chemistry I, Department of Medical Biochemistry and Biophysics, Karolinska Institutet, Stockholm, Sweden.
[3]Division of Pathology, Department of Laboratory Medicine, Karolinska Institutet, Stockholm, Sweden.
[4]Department of Pharmacology and Experimental Neuroscience, University of Nebraska Medical Center, Omaha, NE, United States.
[5]Public Health Agency of Sweden, Solna, Sweden.
[6]Department of Molecular Biology and Umeå Centre for Microbial Research (UCMR), Umeå University, Umeå, Sweden.

[&]Equal contribution
***Corresponding author: Soham Gupta soham.gupta@ki.se**

Running Title: Cellular tropism of SARS-CoV-2

Keywords: SARS-CoV-2, cellular tropism, cytopathogenicity, cell lines, ACE-2, TMPRSS2, Type-I Interferon, proteomics

Abstract

The present pandemic caused by severe acute respiratory syndrome coronavirus-2 (SARS-CoV-2) is driving intense research activities to understand the basic biology of the virus and determine effective therapeutic strategies. The commonly used laboratory cell lines of human origin are the first line of experimental models to study the pathogenicity and performing antiviral assays. Thus, to find suitable cell models to study SARS-CoV-2, we assessed the tropism and cytopathogenicity of the first Swedish isolate of SARS-CoV-2 in six different cell lines of human origin and compared their growth characteristics to other globally isolated strains. Overall, Calu-3, Caco2, Huh7, and 293FT cell lines showed a high to moderate level of susceptibility to the majority of virus isolates. In Caco2 cells the virus can achieve high titers in the absence of any prominent cytopathic effect. The protein expression profile during SARS-CoV-2 infection revealed cell-type-specific regulation of cellular pathways. Type-I interferon signaling was identified as the common dysregulated cellular response in Caco2, Calu-3 and Huh7 cells. Overall, cell-type specific variability was noted for cytopathogenicity, susceptibility and cellular response to SARS-CoV-2. This study provides important clues regarding SARS-CoV-2 pathogenesis and can represent as a guide for future studies to design therapeutics.

48 **Introduction**

49 Severe acute respiratory syndrome coronavirus 2 (SARS-CoV-2), the causative agent of
50 coronavirus disease 2019 (COVID-19) pandemic, is a highly pathogenic coronavirus that has
51 created a global public health challenge (Hu et al., 2020). The virus primarily attacks the lung and
52 the patients often present with severe respiratory distress. However, apart from respiratory
53 symptoms, involvement of other organs with cardiovascular, gastrointestinal, liver, neurological,
54 hematological and skin manifestations in the disease pathology has been documented, suggesting
55 the vulnerability of these anatomical sites to this virus (Gavriatopoulou et al., 2020; Trypsteen et
56 al., 2020). This has been attributed to the presence of the primary receptor of the virus, angiotensin-
57 converting enzyme 2 (ACE2), throughout the body (Hamming et al., 2004). However, we still lack
58 information on the basic virology and the pathogenesis of the virus in different organs.

59 In the current pandemic, numerous research activities have been focusing on understanding the
60 mechanisms of viral pathogenesis and developing effective antivirals against the infection
61 (Appelberg et al., 2020; Bojkova et al., 2020; Chu et al., 2020; Jureka et al., 2020; Zecha et al.,
62 2020). In this scenario, Vero-E6 cell-line has been widely employed for viral isolation, propagation
63 and antiviral testing, due to its high virus production and a prominent cytopathic effect (CPE) upon
64 infection. However, since Vero-E6 originates from monkey and lacks the gene cluster associated
65 with type-I interferon (IFN-I), a more physiologically relevant cell-line of human origin is
66 warranted, that is able to better recapitulate the complexity of host cellular response to the SARS-
67 CoV-2 in humans. Furthermore, the use of cell lines originating from different organs of the body
68 to certain extent can reflect the organ-specific response to the infection and may provide a better
69 understanding of the pathogenesis and transmissibility within body and aid in designing host-
70 targeted therapeutics.

71 In this study, we aimed to determine the SARS-CoV-2 tropism in six commonly used laboratory
72 human cell lines that originate from the lungs, intestine, liver and kidney. Our data provide a
73 comprehensive view of how SARS-CoV-2 behaves differently in different human cell lines
74 depending on the viral strain, the cell line susceptibility and, possibly, the isolation method.
75 Overall, the data presented in this manuscript will be beneficial for choosing a suitable cell system
76 to investigate viral pathogenicity and development therapeutics against SARS-CoV-2.

77

78

Results

Susceptibility and cytotoxicity of first Swedish SARS-CoV-2 isolate in commonly used laboratory cell lines:

We infected Vero-E6, Calu-3, A549, Caco2, Huh7, 293FT and 16HBE with the first Swedish isolate of SARS-CoV-2 virus (SWE/01/2020) at a multiplicity of infection (moi) of 1 and 0.1 as previously described (Appelberg et al., 2020). Virus-induced cytotoxicity was evaluated by measuring the cellular ATP using Viral-ToxGlo™ assay (Promega) and virus production was determined by measuring the presence of viral genome in the cell culture supernatant using qPCR to determine the N-gene RNA (Corman et al., 2020) starting at 3h post-infection (hpi) and followed up to 120hpi (Appelberg et al., 2020). As shown in Figure 1A, infection with moi 0.1 or 1 showed a very similar pattern of virus production over time and by the end of 120h attained similar viral copies in the supernatant. Infection at moi 0.1 induced significant cytopathogenicity in Vero-E6 (less than 3% viability by 48hpi) and a significant increase of 3.8 log10 viral RNA copies in the supernatant at 24hpi. Of the six human cell lines that were tested, Caco2 (intestinal) and polarized Calu-3 (lung) showed the highest virus production with >4 log10 RNA copies by 48hpi ($p<0.001$) and thereafter marginal increase till 120hpi. It was interesting to note that Calu-3 cells, which were infected after 72h of seeding and showed tightly closed together cells with polygonal or cuboidal features and defined boundary, had a higher susceptibility to SARS-CoV-2 compared to Calu-3 cells that were infected after 24h of seeding (round and isolated). The enhanced susceptibility of Calu-3 with longer incubation of 72h prior to infection was possibly due to polarization of the cells (Foster et al., 2000), as was reported previously for SARS-CoV (Tseng et al., 2005). 293FT (kidney; $p<0.01$) and Huh7 (liver; $p<0.02$) showed moderate virus production with >1 log10 viral RNA copies in the supernatant by 120hpi. 16HBE (lung) and A549 (lung) cells showed very poor virus production with <0.6 log10 RNA copies. Interestingly, other than Vero-E6, viral-induced cytotoxicity was only observed in Calu-3 cells with a viability of ≤50% by 48hpi and ≤80% by 72hpi. None of the other cell lines showed any apparent cytotoxicity (viability>85%) (Figure 1B). We observed that the virus production in susceptible cell lines reached saturation by 48hpi. Therefore, we investigated the changes caused in the cell surface of Calu-3, Caco2, Huh7, and 293FT cells during virus production at 48hpi (moi 0.1) using scanning electron microscopy (SEM). We did not observe any significant changes in the morphology of the cell surface in the mock-infected cells. In SARS-CoV-2 infected Calu-3 and Caco2 cells, numerous virus-like particles

110 corresponding to the size of SARS-CoV-2 (approx. 70nM) were observed to be attached to the cell
111 surface or cellular projections (Figure 2A). Interestingly, even though there was moderate virus
112 production in Huh7 and 293FT cells we did not observe any attached virus-like particles on the
113 cell surface after scanning several fields (data not shown). The possible reasons for this could be
114 either low level virus production in Huh7 cells and 293FT cells compared to Calu-3 and Caco2
115 cells that was missed visually or the virus release mechanism is different than the budding out of
116 the virus (Ghosh et al., 2020).
117
118 **Expression of ACE2 and TMPRSS2 in different cell lines:**
119 ACE2 receptor and transmembrane serine protease 2 (TMPRSS2) activity have been shown to be
120 critical for SARS-CoV-2 entry into the cell (Jureka et al., 2020; Matsuyama et al., 2020). To
121 correlate the ACE2 and TMPRSS2 expression with the tropism, we determined the protein
122 expression in the cell lysates by western blot (Figure 2B). Among the infected cell lines, ACE2
123 expression was only observed in Vero-E6, Calu-3 and Caco2 that correlated with high virus
124 production. When we looked into co-expression of ACE2 and TMPRSS2, it was most prominent
125 in Caco2, followed by Vero-E6 and Calu-3, although Calu-3 showed low TMPRSS2 expression.
126 Contrarily, Huh7 and 293FT strongly expressed TMPRSS2 but lacked ACE2 expression indicating
127 that each receptor has an individual role in aiding the infection.
128
129 **Susceptibility and cytopathogenicity of globally isolated SARS-CoV-2 strains:**
130 To compare the tropism of the Swedish SARS-CoV-2 virus with the other globally isolated strains,
131 we performed a literature survey to determine the susceptibility and cytopathogenicity in all the
132 six cell lines as noted above. We have included virus isolates from Germany (FFM1/2020
133 (Bojkova et al., 2020) and Mun_IMB1/2020 (Zecha et al., 2020)), France (IHUMI2) (Wurtz et al.,
134 2020), USA (WA1/2020) (Jureka et al., 2020), Canada (SB3-TYAGNC) (Banerjee et al., 2020),
135 China (KMS1/2020) (Liao et al., 2020), Hong Kong (HKU-001a/2020 (Chu et al., 2020) and
136 VM20001061/2020 (Hui et al., 2020), Taiwan (NTU01/2020 and NTU02/2020) (Hsin et al., 2020)
137 and Japan (TY-WK-521/2020) (Matsuyama et al., 2020) and found major differences in cellular
138 tropism and cytopathogenicity (Figure 2C). Specifically, we observed that the majority of the
139 strains were able to infect both Caco2 and Calu-3, except for the Muc_IMB1/2020 (both the cell
140 lines not susceptible) (Zecha et al., 2020) and the Japanese strain (Calu-3 cells not susceptible)

141 (Matsuyama et al., 2020). The Frankfurt_FFM1/2020 strain showed a rapid CPE in Caco2 by 24hpi
142 at moi 0.1 (Bojkova et al., 2020), while other strains, including the Swedish isolate, did not show
143 any prominent CPE either at higher infective dose or with prolonged time of incubation (Chu et
144 al., 2020). Additionally, using the Wuhan/Hu-1/2019 strain as reference, we compared the amino
145 acid changes in the spike protein of these strains. The Frankfurt and Taiwan strains showed no
146 dissimilarities, while the Swedish (F797C), Munich (D614G), China (N74K) and Hong Kong
147 (V367F) strains each showed a single amino acid substitution (Figure 2D).
148
149 **Proteomic analysis of the cell lines:**
150 Since we observed differential susceptibility to SARS-CoV-2 infection in different cell lines
151 originating from the human lung (Calu-3), intestine (Caco2), liver (Huh7) and kidney (293FT), we
152 investigated how the cellular proteins are regulated during infection in these cell lines. To this end,
153 we either infected or mock-infected polarized Calu-3 cells, Caco2 cells, Huh7 cells and 293FT
154 cells with SARS-CoV-2 (moi 1) in triplicates. The cells were harvested 24hpi, lysed and equal
155 concentration of the protein was used to perform quantitative proteomics using a TMT-labeling
156 strategy as previously described (Appelberg et al., 2020). Among the four cell lines, Calu-3
157 showed major changes in protein abundance upon infection, with 6462 proteins differentially
158 expressed in infected cells than the mock, followed by Caco2 with a significant difference in 177
159 proteins. No change in the global protein abundance was observed in Huh7 (only four proteins
160 differentially expressed) and 293FT (no proteins differentially expressed) at 24hpi (Figure 3A,
161 Supplemental Table S3). The virus secretion in the cell culture supernatant at 3hpi and 24hpi is
162 shown in Figure 3B. The viral protein abundance in the cells is shown in Figure 3C. The proteins
163 that were detected are ORF3a, ORF6, ORF7a, ORF8, ORF9b, M, N, S and Replicase polyprotein
164 1ab (abbreviated as rep). The higher abundance of viral proteins detected in Calu-3 correlated with
165 higher level of virus production and the change in host protein abundance.
166
167 **Type-I IFN signaling is commonly dysregulated in Calu-3, Caco2 and Huh7 cell lines by**
168 **SARS-CoV-2:**
169 Since Calu-3 and Caco2 were the only cell lines that showed substantial protein regulation upon
170 infection at 24h, we compared the significantly regulated proteins in those two cell lines. As shown
171 in the Venn diagram in Figure 4A, there were 132 proteins that were commonly dysregulated in

172 both Calu-3 and Caco2. Among the 132 dysregulated proteins, 88 proteins were similarly
173 upregulated (44 proteins) and downregulated (44 proteins) in both the cell lines (Supplemental
174 figure S1). Reactome pathway analysis on the 132 significantly altered proteins common to both
175 cell lines showed a strong enrichment of type-I and type-II interferon signaling pathways and its
176 related RIG-I/MDA5 (DDX58/IFIH1) signaling pathway (Figure 4B). To investigate which are
177 the proteins associated with this pathway changing upon infection, as a next step, we assessed the
178 changes induced by the infection in the levels of each protein associated with the following
179 pathways: interferon response, including the interferon alpha/beta signaling (Pathway: R-HSA-
180 909733), interferon gamma signaling (Pathway: R-HSA-877300) and antiviral mechanism by
181 IFN-stimulated genes (ISGs, Pathway: R-HSA-1169410). As shown in the heatmaps, 105 (out of
182 129 detected) and 27 (out of 131 detected) were differentially regulated in Calu-3 (Figure 4C,
183 Supplemental Table S4), and Caco2 respectively (Figure 4D, Supplemental Table S4). At 24hpi,
184 both 293FT and Huh7 did not show any differentially regulated protein belonging to IFN-signaling
185 pathways (109 detected proteins; Supplemental Table S4) and the heat maps are shown in
186 Supplemental Figure S2. As shown in the heatmaps, among 129 detected proteins belonging to
187 these pathways, 105 were differentially regulated in Calu-3 (63 upregulated and 42
188 downregulated), while in Caco2 among 131 detected proteins 27 were differentially regulated (25
189 upregulated and 2 downregulated) (Figure 4C and 4D, Supplemental Table S4). The protein-
190 protein interaction network of the significantly altered proteins showed two definite clusters in
191 Calu-3: one including proteins associated with RIG-I (DDX58) and Type-I/II signaling complex
192 and another majorly including components of nucleoporin complex that were down-regulated. The
193 karyopherin family, and a single cluster (RIG-I (DDX58) and Type-I signaling complex) were
194 upregulated in Caco2 (Supplemental Figure S3A and S3B). In general, we observed an interferon
195 stimulation in SARS-CoV-2 infected Calu-3 and Caco2 cells and SARS-CoV-2 receptor ACE2
196 has been considered to be an interferon stimulatory gene (Ziegler et al., 2020). However, we did
197 not observe any significant differences in the protein levels of ACE2 or TMPRSS2 upon infection
198 in our proteomics data, rather ACE2 was down-regulated in SARS-CoV-2 infected cells
199 (Supplemental Figure S4).
200 Type-I IFN, like IFN-β, plays a major role in host defenses against various viruses and in our
201 proteomics data we observed dysregulation of type-I IFN response associated proteins including
202 ISGs, therefore we assessed the mRNA expression of IFN-β and the downstream ISGs (IFIT1,

203 MX1, MX2, ISG15 and RIG-I) using qPCR. In line with our proteomics findings, the mRNA
204 levels of IFN-β and all the tested ISGs significantly increased upon SARS-CoV-2 infection in
205 Calu-3 and Caco2 cells. 293FT and Huh7 cells did not show any significant variations at 24hpi
206 (Figure 5A). IFN-β is released by cells through a signaling cascade that is initiated after activation
207 of RIG-I or RLRs upon interaction with viral products. The western blot analysis showed a major
208 increase in activation of RIG-I, MDA-5 and its downstream effectors p-IRF3, p-STAT1 and ISG15
209 in infected Calu-3 and Caco2 cells (Figure 5B and 5C) corroborating the qPCR results. In general,
210 the steady-state level of RIG-I, MDA-5 and ISG15 were higher in Caco2 and Calu-3 cells as
211 compared to 293FT and Huh7 cells and the latter two showing no comparable changes following
212 24hpi (Figure 5C). No observable change was noted in conjugated ISG15 in any of the cell lines
213 (Supplemental Figure S5A and S5B). It is conceivable that the observed changes in SARS-CoV-2
214 infected Calu-3 and Caco2 cells 24hpi could be due to high level of infectivity as observed by the
215 expression of SARS-CoV-2 nucleoprotein (Figure 5B and 5C) and higher susceptibility (Figure
216 1B and 3B) as compared to 293FT and Huh7.
217 Previous proteomics-based studies have observed that SARS-CoV-2 causes global proteomic
218 changes after 48hpi specifically in pathways related to ErbB, HIF-1, mTOR and TNF signaling
219 (Appelberg et al., 2020), complement system and coagulation cascades (Tiwari et al., 2020) and
220 interferon signaling (Unpublished data). In order to understand the delayed changes in Huh7 cells
221 ($Huh7^{48h}$) compared to Calu-3 and Caco2 cells, we extracted the proteomics data set from our
222 earlier study (Appelberg et al., 2020). Next, we aligned the significantly changed proteins in this
223 data set with that of the Calu-3 and Caco2 cells. There were 42 common proteins that were
224 dysregulated in all three cell lines (Figure 6A), showing similar trend in 15 proteins (8 were
225 commonly upregulated and 7 were commonly downregulated) and opposite trends in 27 proteins
226 in all the three cell lines (Supplemental Figure S6). We employed Reactome pathway analysis to
227 define the commonly dysregulated pathways using 42 proteins and observed that pathways related
228 to interferon signaling were the top hits (Figure 6B). We looked in detail into the 24 proteins that
229 belonged to pathways related to IFN-signaling and were significantly altered in Calu-3 and Caco2.
230 As shown in Figure 6C, only STAT2, STAT1, DDX58, ISG15 and IFIT1 were commonly
231 upregulated in all three cell lines. Distinct features were noticed in B2M, PML, HLA-E and HLA-
232 B in Calu-3 (downregulated), Caco2 (upregulated) and $Huh7^{48h}$ (no change). IFI35 was
233 upregulated in both Calu-3 and Caco2 cells but was downregulated in $Huh7^{48h}$.

234

235 **Cell-type and virus specific differences in proteome:**

236 There are obvious commonalities and distinct features between different cell lines that could be
237 defined by the tissue of origin. Till now we have shown that SARS-CoV-2 commonly regulates
238 the type-I IFN signaling in cell lines derived from different tissues. In order to determine which
239 other pathways are distinctively regulated by SARS-CoV-2 in Calu-3, Caco2 and Huh7^{48h} cells,
240 we identified the proteins that were significantly uniquely altered by infection in each of the 3 cell
241 lines. There were 3897 proteins in Calu-3, 1347 proteins in Huh7^{48h} and 38 proteins in Caco2 that
242 uniquely changed (Figure 6A). A Reactome pathway analysis on these proteins revealed major
243 changes in pathways related to mitochondrial processes in Calu-3 (Supplemental Figure S7A), and
244 eukaryotic translation processes in Huh7^{48h} (Supplemental Figure S7B). We could not identify
245 clearly any specific pathway modulated in Caco2. Additionally, we investigated altered pathways
246 shared between only Huh7^{48h} and Caco2 and only Huh7^{48h} and Calu-3. As presented in
247 Supplemental Figures S8A and S8B respectively, unlike Caco2 and Calu-3 they did not show
248 shared characteristics of IFN-signaling dysregulation as top pathways.

249

250

251 **Discussion**

252 Cellular models that reproduce the SARS-CoV-2 life cycle are essential to understand the viral-
253 host interplay and to test new antivirals. Vero-E6 cell-line that originates from African green
254 monkey kidney cells is often a choice for cell culture-based infection model for coronavirus
255 research (Ogando et al., 2020), since it expresses the receptor ACE2 and shows prominent
256 cytopathogenicity with efficient virus production. However, Vero-E6 may not be a suitable cell
257 model to study the pathophysiology of the cell in response to the virus infection as it lacks genes
258 encoding type-I interferons (Osada et al., 2014). Cell lines of human origin are more relevant. In
259 the present study, we systematically analyzed SARS-CoV-2 susceptibility and cytopathogenicity
260 in cell lines originating from human lung (Calu-3, A549, 16HBE), colon (Caco2), liver (Huh7)
261 and kidney (293FT). Furthermore, using proteomics we characterized the cellular changes caused
262 by SARS-CoV-2 in the susceptible cell lines Calu-3, Caco2, 293FT and Huh7. Our data provides
263 insight into the cell-type-specific cellular re-organization caused by SARS-CoV-2.

264 Several recent studies testing different local strains show conflicting results concerning
265 susceptibility and cytopathogenicity in human cell lines (Figure 2C), mostly when Caco2 and
266 Calu-3 cells are employed. The Swedish isolate tested here showed high virus production and
267 prominent cytopathogenicity in Calu-3 cells. However, it needs to be pointed out that the
268 susceptibility of the Calu-3 cells increased following polarization of the cells after 72h of
269 incubation before infection, as with 24h of incubation of the cells prior to infection showed a very
270 moderate virus production and a delayed CPE (Figure 1). Another observation with Calu-3 cells
271 was that upon infection, they did not show a CPE similar to Vero-E6; rather the Calu-3 stopped
272 growing, rounded up and mottled, as compared to the uninfected control. The morphological
273 change observed in Calu-3 might represent a cellular mechanism to control viral infection and
274 therefore requires more investigation. Several other studies did not align with our findings as the
275 strain from Munich (Zecha et al., 2020) and Japan (Matsuyama et al., 2020) showed very poor
276 susceptibility and the Hong Kong strain showed a high susceptibility with no cytopathogenicity
277 (Chu et al., 2020; Hui et al., 2020). The discrepant susceptibility could be dependent on the
278 polarization of the Calu-3 cells where ACE2, the receptor for SARS-CoV-2, is expressed apically
279 in polarized Calu-3 cells and has been shown to facilitate entry and release of the SARS-CoV
280 (Tseng et al., 2005). Caco2 was another cell line that showed varied level of susceptibility in
281 different studies. In Caco2 while we observed high viral susceptibility, we did not observe any
282 appreciable cytopathogenicity as was reported for the French (Wurtz et al., 2020) and the Honk
283 Kong strain (Chu et al., 2020). Bojkova et al. have performed a time-course proteomic study in
284 with the Frankfurt strain of SARS-CoV-2 in infected Caco2 cells over a period of 24h (Bojkova et
285 al., 2020). Contrary to our results (Figure 1), the authors observed cytopathogenicity in Caco2 cells
286 24hpi. In order to compare their 24hpi proteomic data with ours we re-analyzed their data with
287 similar statistical considerations as ours. Compared to ours, they observed a very high number of
288 proteins to be significantly altered (1379 vs 177), among which we observed only 30 proteins
289 overlapping in both studies (Figure 7A). A heatmap of the 30 common proteins over time in the
290 Bojkova et al. data is shown in Figure 7B and the heatmap of the same proteins in our study at
291 24hpi is shown in Figure 7C. We observed discordance in 4 proteins, where TTR and IFI35 were
292 upregulated in their study but downregulated in ours and ITGB4 and LYPD3 were downregulated
293 in their study but were upregulated in ours. We also specifically looked into the proteins related to
294 IFN-signaling pathways and observed several nuclear transporters to be upregulated in the

295 Bojkova et al. study. Among the ISGs, only ISG15 showed an upregulation in both the data
296 (Supplemental Figure S9). Of note, unlike others, the Frankfurt strain was the only strain that was
297 isolated and adapted in Caco2 that could have possibly led to higher susceptibility and CPE of this
298 strain in the cell-line (Bojkova et al., 2020). In addition, different infective doses, structural
299 changes in the virus, culture conditions and clonal differences in the cell lines could also govern
300 strain-specific differences in cellular tropism of SARS-CoV-2.
301 A major role in susceptibility to viral infection is played by the interaction between viral envelope
302 glycoproteins and cellular receptors, which initiate the early phases of the viral life cycle.
303 Therefore, we first investigated whether mutations in the spike glycoproteins of the different
304 strains presented above could affect their tropism and cytopathogenicity. However, no major
305 amino acid changes were observed in the spike protein, except for the Munich strain harboring
306 D614G mutation that had become the dominant genotype in Europe and considered to be more
307 infectious in humans (Korber et al., 2020). Interestingly, both Caco2 and Calu-3 were not
308 susceptible to the Munich strain in the study performed by Zecha et al. and this correlated with the
309 absence of ACE2 expression in their steady-state proteomics data obtained from Caco2 and Calu-
310 3 cell lines (Zecha et al., 2020). ACE2 and TMPRSS2 proteins are considered essential for SARS-
311 CoV-2 entry and ACE2 expression alone strongly correlated with the virus susceptibility. We
312 observed a strong correlation between ACE2 expression and virus tropism, while increased
313 expression of TMPRSS2 alone in Huh7 and 293FT cell lines showed susceptibility to SARS-CoV-
314 2, perhaps due to TMPRSS2 mediated enhanced virus uptake into the cell (Heurich et al., 2014).
315 However, we cannot exclude the possibility that other molecules or endocytosis mechanisms are
316 involved in viral recognition and entry.
317 In addition, in the present study, we have investigated the replicative capacity of the virus by
318 measuring the presence of newly produced virions in the culture supernatant. Another interesting
319 observation was that we did not observe any virus budding in the cell surface of Huh7 and 293FT,
320 in spite of increased viral RNA in the supernatant over time, differently from Caco2 and Calu-3
321 (Figure 2). Recently, it has been shown that beta-coronaviruses can hijack the lysosomal organelles
322 resulting in non-lytic exocytosis of the virus (Ghosh et al., 2020). Overall our data on SARS-CoV-
323 2 virus production, release, receptor expression and cytotoxicity highlight the cell-line specific
324 SARS-CoV-2 life cycle and suggest different mechanisms of remodeling of the host cellular
325 environment during infection, which we addressed by quantitative proteomics. While there were

326 definite virus-specific proteome changes (Supplemental Figure S7), the pathways that were
327 commonly regulated between Caco2 and Calu-3 belonged to type-I interferon signaling. It was
328 also evident that the dynamics of the viral life cycle influences the proteomic landscape or vice
329 versa. As, in Caco2 and Calu-3 an efficient production of the virus correlated with increased
330 activation of RIG-I/MDA5 signaling and subsequently IFN-β and ISGs by 24hpi (Figure 4 and 5).
331 However, this was not observed in 293FT and Huh7. In another study, we have observed that in
332 Huh7 cells SARS-CoV-2 can inhibit type-I IFN signaling early and the dysregulation in this
333 pathway is only observed 48hpi (unpublished data), which correlates with moderate production of
334 the virus. In spite of differences in the dynamics of the cellular response, type-I IFN pre-
335 sensitization of the Caco2, Calu-3 (Shuai et al., 2020) and Huh7 (unpublished data) has been shown
336 to effectively inhibit SARS-CoV-2 infection. Additionally, many of the ISGs like IFIT1, ISG15
337 and DDX58 were upregulated in all the three cell lines (Figure 6). These findings suggest that even
338 in presence of cell-type specific diversity in cellular responses, there are common pathways that
339 could be efficiently targeted to inhibit SARS-CoV-2. This is particularly relevant since SARS-
340 CoV-2 can infect different organs of the body (Mallapaty, 2020; Trypsteen et al., 2020).
341 One limitation of our study is that the analysis is restricted to cell lines, which may not be
342 physiologically representative of the human tissue, contrary to organoids, but we still provide an
343 overview of the complexity and variability of the interaction between SARS-CoV2 and the human
344 cellular targets. Furthermore, we restricted our proteomics study to 24hpi and more detailed time
345 kinetics experiments are required to elucidate better the dynamic changes occurring during
346 infection.
347 In conclusion, we identify several cell lines of human origin that could be used as physiologically
348 relevant cell models to study the biological properties of SARS-CoV-2. Type-I interferon is
349 commonly regulated during infection in cell lines originating from lungs, colon and liver and
350 warrants more mechanistic studies to identify factors that could be utilized to control the infection.
351
352
353
354
355
356

357 **Figure Legends:**

358 **Figure 1. Viral production and cytopathogenicity of SARS-CoV-2 in Vero E6 and six**
359 **different cell lines of human origin.** Indicated cell lines were infected with SARS-CoV-2 at moi
360 of 1 and 0.1 either in duplicate or triplicate. A. Viral supernatant samples were harvested at 3hpi,
361 24hpi, 48hpi, 72hpi, 96hpi and 120hpi. Viral production was determined by quantitative qRT-PCR
362 targeting the N gene of SARS-CoV-2 comparing each time points to 3hpi. B. Cell viability was
363 measured at 3h post infection (hpi), 24hpi, 48hpi, 72hpi, 96hpi and 120hpi by Viral-ToxGlo™
364 assay. The viability at each time was determined in comparison to the uninfected control.

365 **Figure 2**. **Cell-specific and strain-specific differences in SARS-CoV-2 tropism.** A. Scanning
366 electron microscopy images of the cell surface of mock-infected and SARS-CoV-2 infected (moi
367 0.1) Caco2 and Calu-3 cells. Indicated cell lines were infected with SARS-CoV-2 at an moi of 0.1
368 and fixed 48hpi for microscopy analysis. B. ACE2 and TMPRSS2 receptor expression in six
369 human cell lines. ACE2 and TMPRSS2 expression in these cell lines were determined by western
370 blot in the cell lysates. Heatmaps with relative protein quantification (blue), susceptibility (orange)
371 and cytotoxicity (green) are shown. C. Susceptibility of globally isolated SARS-CoV-2 strains.
372 Based on previously published or preprint articles, a chart was created showing the susceptibility
373 of the commonly used laboratory cell lines and cytopathogenicity of SARS-CoV-2 strains isolated
374 from different geographical locations. Boxes are color coded based on intensity as indicated in the
375 figure. The moi used wherever available is mentioned in the bottom. D. Table showing presence
376 of any amino acid substitution in the spike protein of the indicated strains. NA= Not available.

377 **Figure 3. Proteomic landscape of different commonly used laboratory cell lines upon SARS-**
378 **CoV-2 infection.** A. Brief methodology of the proteomics experiment in the indicated cell lines
379 that were either mock-infected or infected with SARS-CoV-2 moi 1 for 24h. Significantly altered
380 host proteins in the indicated cell lines are represented in the heatmap. B. Relative viral production
381 in the cell supernatant, measured at 3hpi and 24hpi. C. Detected viral proteins in the indicated cells
382 by tandem mass tag-labeled mass spectrometry (TMT-MS).

383 **Figure 4. Interferon-signaling pathways are commonly dysregulated by SARS-CoV-2**
384 **infection in Caco2 and Calu-3 cell lines.** A. Venn diagram and overlap of proteins with
385 significant abundance between mock and 24hpi in Caco2 and Calu-3 cell lines. B. Barplot
386 enrichment map of significant overlapping proteins in Caco2 and Calu-3 cell lines from
387 ReactomePA. Number of proteins are indicated on the x axis. P values are indicated from highly

388 significant in red to significant in blue. C. Heatmap representing the number of significant proteins
389 (LIMMA, FDR < 0.05) between mock and 24hpi in Calu-3 cell line. D. Heatmap representing the
390 number of significant proteins (LIMMA, FDR < 0.05) between mock and 24hpi in Caco2 cell line.
391 **Figure 5. Different expression of ISGs in the infected cell lines.** A. The gene expression level
392 of IFN-β and indicated representative interferon stimulated genes (ISGs): IFIT1, MX2, MX1,
393 ISG15 and RIG-I in Calu-3, Caco2, 293FT and Huh7 cell lines 24hpi. The results are shown as
394 fold change relative to mock-infected cells, normalized to GAPDH. The mean ± SEM of at least
395 two independent experiments is shown. M = mock; V = virus. B. Protein expression levels of
396 MDA-5, RIG-I, pIRF-3, p-STAT1, and viral nucleocapsid in infected and mock-infected Calu-3,
397 Caco2, 293FT and Huh7 cells 24hpi. C. The intensity of specific bands for MDA-5, RIG-I, mono-
398 ISG15 and SARS-CoV-2 nucleoprotein was quantified by ImageJ and fold change was calculated
399 relative to the mock-infected cells, normalized to β-actin. The intensity of p-IRF3 and p-STAT1
400 was not quantified as expression could be observed only in one of the experimental replicates. The
401 mean ± SEM of at least two experiments is shown.
402 **Figure 6. Overlap of three cell lines confirm the implication of interferon pathway in SARS-**
403 **CoV-2 infection.** A. Venn diagram and overlap of proteins with significant abundance between
404 mock and 24hpi in Caco2, Calu-3 and Huh7 cell lines. B. ClusterProfiler enrichment map of
405 significant proteins in Caco2, Calu-3 and Huh7 cell lines. Size of the bubble is proportional to
406 gene ratio. C. ReactomePA barplot enrichment map of significant overlapping proteins in Caco2,
407 Calu-3 and Huh7 cell lines.
408 **Figure 7. Validation of proteins dysregulated in Caco2 cell lines by SARS-CoV-2 infection**
409 **from independent studies.** A. Venn diagram and overlap of proteins with significant abundance
410 between mock and 24hpi in Caco2 cell lines from this study and a study by Bojkova et al. B.
411 Heatmap of significant overlapping proteins in mock-infected and SARS-CoV-2 infected cells at
412 24h in Bojkova et al. Data were quantile normalized and Z-score transformed. Lower values are
413 represented in yellow and higher values in purple. Significant differentially expressed proteins
414 between time points are indicated in blue if downregulated and in red if up-regulated. C. Heat map
415 of the significant differentially abundant proteins of the Bojkova et al. in our dataset (Bojkova et
416 al., 2020).
417
418

Acknowledgments:

We would like to thank Prof. Lena Palmberg, and Asst. Prof. Swapna Upadhyay, Karolinska Institute for providing the 16HBE cell line and Prof. Matti Sällberg for providing the 293FT cells. The authors would like to acknowledge the support from the Proteomics Biomedicum, Karolinska Institutet for LC-MS/MS analysis. The study is funded by Swedish Research Council Grants (2017-01330) to U.N., Karolinska Institute Stiftelser och Fonder (2020-02153 to S.G. and 2020-01554 to U.N.), Åke Wibergs Stiftelse (M20-0220) to S.G., Swedish research Council (2018-05766 and 2017-03126) and Innovative Medicines Initiative 2 Joint Undertaking (JU) under grant agreement no. 101005026 to A.M. JU receives support from the European Union's Horizon 2020 research and innovation programme and EFPIA. TF acknowledges the grant received from the Swedish Cancer Society and the Swedish Research Council.

Authors Contribution:

E.S. designed the experiments, performed experimental work, analyzed the results and wrote the first draft of the manuscript**. X.C.** performed experimental work, analyzed the results and reviewed and edited the manuscript. **F.M.** performed the bioinformatics analysis and wrote the first draft of the manuscript. **Á.V.** and **J.E.R.** performed the mass-spectrometry and reviewed and edited the manuscript. **L.S.** performed the electron microscopy. **B.S.V.** and **S.K.** performed experimental work and reviewed and edited the manuscript. **T.F.** and **S.N.B** .provided intellectual content and reviewed and edited the manuscript. **A.M.** contributed with resources, intellectual content and reviewed and edited the manuscript. **U.N.** conceptualized, acquired funding, provided intellectual content and reviewed and edited the manuscript. **S.G.** conceptualized, supervised and performed the experimental work, analyzed the results, acquired funding, and wrote the manuscript together with all the co-authors. All authors have read and agreed to the published version of the manuscript.

Competing interests:

The authors declare no competing interests.

Data availability:

All data generated or analyzed during this study are included in this published article. Information regarding any additional data are available from the corresponding author on reasonable request.

450 **References:**

451 Appelberg, S., Gupta, S., Svensson Akusjarvi, S., Ambikan, A.T., Mikaeloff, F., Saccon, E.,
452 Vegvari, A., Benfeitas, R., Sperk, M., Stahlberg, M., *et al.* (2020). Dysregulation in
453 Akt/mTOR/HIF-1 signaling identified by proteo-transcriptomics of SARS-CoV-2 infected cells.
454 Emerging microbes & infections *9*, 1748-1760.

455 Banerjee, A., Nasir, J.A., Budylowski, P., Yip, L., Aftanas, P., Christie, N., Ghalami, A., Baid, K.,
456 Raphenya, A.R., Hirota, J.A., *et al.* (2020). Isolation, Sequence, Infectivity, and Replication
457 Kinetics of Severe Acute Respiratory Syndrome Coronavirus 2. Emerging infectious diseases *26*,
458 2054-2063.

459 Bojkova, D., Klann, K., Koch, B., Widera, M., Krause, D., Ciesek, S., Cinatl, J., and Munch, C.
460 (2020). Proteomics of SARS-CoV-2-infected host cells reveals therapy targets. Nature *583*, 469-
461 472.

462 Chu, H., Chan, J.F., Yuen, T.T., Shuai, H., Yuan, S., Wang, Y., Hu, B., Yip, C.C., Tsang, J.O.,
463 Huang, X., *et al.* (2020). Comparative tropism, replication kinetics, and cell damage profiling of
464 SARS-CoV-2 and SARS-CoV with implications for clinical manifestations, transmissibility, and
465 laboratory studies of COVID-19: an observational study. Lancet Microbe *1*, e14-e23.

466 Corman, V.M., Landt, O., Kaiser, M., Molenkamp, R., Meijer, A., Chu, D.K., Bleicker, T.,
467 Brunink, S., Schneider, J., Schmidt, M.L., *et al.* (2020). Detection of 2019 novel coronavirus
468 (2019-nCoV) by real-time RT-PCR. Euro surveillance : bulletin Europeen sur les maladies
469 transmissibles = European communicable disease bulletin *25*.

470 Foster, K.A., Avery, M.L., Yazdanian, M., and Audus, K.L. (2000). Characterization of the Calu-
471 3 cell line as a tool to screen pulmonary drug delivery. International journal of pharmaceutics *208*,
472 1-11.

473 Gavriatopoulou, M., Korompoki, E., Fotiou, D., Ntanasis-Stathopoulos, I., Psaltopoulou, T.,
474 Kastritis, E., Terpos, E., and Dimopoulos, M.A. (2020). Organ-specific manifestations of COVID-
475 19 infection. Clinical and experimental medicine *20*, 493-506.
476 Ghosh, S., Dellibovi-Ragheb, T.A., Kerviel, A., Pak, E., Qiu, Q., Fisher, M., Takvorian, P.M.,
477 Bleck, C., Hsu, V.W., Fehr, A.R.*, et al.* (2020). β-Coronaviruses Use Lysosomes for Egress Instead
478 of the Biosynthetic Secretory Pathway. Cell *183*, 1520-1535 e1514.
479 Hamming, I., Timens, W., Bulthuis, M.L., Lely, A.T., Navis, G., and van Goor, H. (2004). Tissue
480 distribution of ACE2 protein, the functional receptor for SARS coronavirus. A first step in
481 understanding SARS pathogenesis. The Journal of pathology *203*, 631-637.
482 Heurich, A., Hofmann-Winkler, H., Gierer, S., Liepold, T., Jahn, O., and Pohlmann, S. (2014).
483 TMPRSS2 and ADAM17 cleave ACE2 differentially and only proteolysis by TMPRSS2 augments
484 entry driven by the severe acute respiratory syndrome coronavirus spike protein. Journal of
485 virology *88*, 1293-1307.
486 Hsin, F., Chao, T.-L., Chan, Y.-R., Kao, H.-C., Liu, W.-D., Wang, J.-T., Pang, Y.-H., Lin, C.-H.,
487 Tsai, Y.-M., Lin, J.-Y.*, et al.* (2020). Distinct Inductions of and Responses to Type I and Type III
488 Interferons Promote Infections in Two SARS-CoV-2 Isolates. bioRxiv.
489 Hu, B., Guo, H., Zhou, P., and Shi, Z.L. (2020). Characteristics of SARS-CoV-2 and COVID-19.
490 Nature reviews Microbiology, 1-14.
491 Hui, K.P.Y., Cheung, M.C., Perera, R., Ng, K.C., Bui, C.H.T., Ho, J.C.W., Ng, M.M.T., Kuok,
492 D.I.T., Shih, K.C., Tsao, S.W.*, et al.* (2020). Tropism, replication competence, and innate immune
493 responses of the coronavirus SARS-CoV-2 in human respiratory tract and conjunctiva: an analysis
494 in ex-vivo and in-vitro cultures. The Lancet Respiratory medicine *8*, 687-695.

495 Jureka, A.S., Silvas, J.A., and Basler, C.F. (2020). Propagation, Inactivation, and Safety Testing
496 of SARS-CoV-2. Viruses *12*.
497 Korber, B., Fischer, W.M., Gnanakaran, S., Yoon, H., Theiler, J., Abfalterer, W., Hengartner, N.,
498 Giorgi, E.E., Bhattacharya, T., Foley, B.*, et al.* (2020). Tracking Changes in SARS-CoV-2 Spike:
499 Evidence that D614G Increases Infectivity of the COVID-19 Virus. Cell *182*, 812-827 e819.
500 Liao, Y., Li, X., Mou, T., Zhou, X., Li, D., Wang, L., Zhang, Y., Dong, X., Zheng, H., Guo, L.*, et*
501 *al.* (2020). Distinct infection process of SARS-CoV-2 in human bronchial epithelial cells line.
502 Journal of medical virology.
503 Mallapaty, S. (2020). Mini organs reveal how the coronavirus ravages the body. Nature *583*, 15-
504 16.
505 Matsuyama, S., Nao, N., Shirato, K., Kawase, M., Saito, S., Takayama, I., Nagata, N., Sekizuka,
506 T., Katoh, H., Kato, F.*, et al.* (2020). Enhanced isolation of SARS-CoV-2 by TMPRSS2-
507 expressing cells. Proceedings of the National Academy of Sciences of the United States of America
508 *117*, 7001-7003.
509 Ogando, N.S., Dalebout, T.J., Zevenhoven-Dobbe, J.C., Limpens, R., van der Meer, Y., Caly, L.,
510 Druce, J., de Vries, J.J.C., Kikkert, M., Bárcena, M.*, et al.* (2020). SARS-coronavirus-2 replication
511 in Vero E6 cells: replication kinetics, rapid adaptation and cytopathology. The Journal of general
512 virology *101*, 925-940.
513 Osada, N., Kohara, A., Yamaji, T., Hirayama, N., Kasai, F., Sekizuka, T., Kuroda, M., and Hanada,
514 K. (2014). The genome landscape of the african green monkey kidney-derived vero cell line. DNA
515 research : an international journal for rapid publication of reports on genes and genomes *21*, 673-
516 683.

517 Shuai, H., Chu, H., Hou, Y., Yang, D., Wang, Y., Hu, B., Huang, X., Zhang, X., Chai, Y., Cai,
518 J.P., *et al.* (2020). Differential immune activation profile of SARS-CoV-2 and SARS-CoV
519 infection in human lung and intestinal cells: Implications for treatment with IFN-β and IFN
520 inducer. The Journal of infection *81*, e1-e10.
521 Tiwari, R., Mishra, A.R., Mikaeloff, F., Gupta, S., Mirazimi, A., Byrareddy, S.N., Neogi, U., and
522 Nayak, D. (2020). In silico and in vitro studies reveal complement system drives coagulation
523 cascade in SARS-CoV-2 pathogenesis. Computational and structural biotechnology journal *18*,
524 3734-3744.
525 Trypsteen, W., Van Cleemput, J., Snippenberg, W.V., Gerlo, S., and Vandekerckhove, L. (2020).
526 On the whereabouts of SARS-CoV-2 in the human body: A systematic review. PLoS pathogens
527 *16*, e1009037.
528 Tseng, C.T., Tseng, J., Perrone, L., Worthy, M., Popov, V., and Peters, C.J. (2005). Apical entry
529 and release of severe acute respiratory syndrome-associated coronavirus in polarized Calu-3 lung
530 epithelial cells. Journal of virology *79*, 9470-9479.
531 Wurtz, N., Penant, G., Jardot, P., Duclos, N., and La Scola, B. (2020). Culture of SARS-CoV-2 in
532 a panel of laboratory cell lines. IHU.
533 Zecha, J., Lee, C.Y., Bayer, F.P., Meng, C., Grass, V., Zerweck, J., Schnatbaum, K., Michler, T.,
534 Pichlmair, A., Ludwig, C., *et al.* (2020). Data, Reagents, Assays and Merits of Proteomics for
535 SARS-CoV-2 Research and Testing. Mol Cell Proteomics *19*, 1503-1522.
536 Ziegler, C.G.K., Allon, S.J., Nyquist, S.K., Mbano, I.M., Miao, V.N., Tzouanas, C.N., Cao, Y.,
537 Yousif, A.S., Bals, J., Hauser, B.M., *et al.* (2020). SARS-CoV-2 Receptor ACE2 Is an Interferon-
538 Stimulated Gene in Human Airway Epithelial Cells and Is Detected in Specific Cell Subsets across
539 Tissues. Cell *181*, 1016-1035 e1019.

540

Figure 1

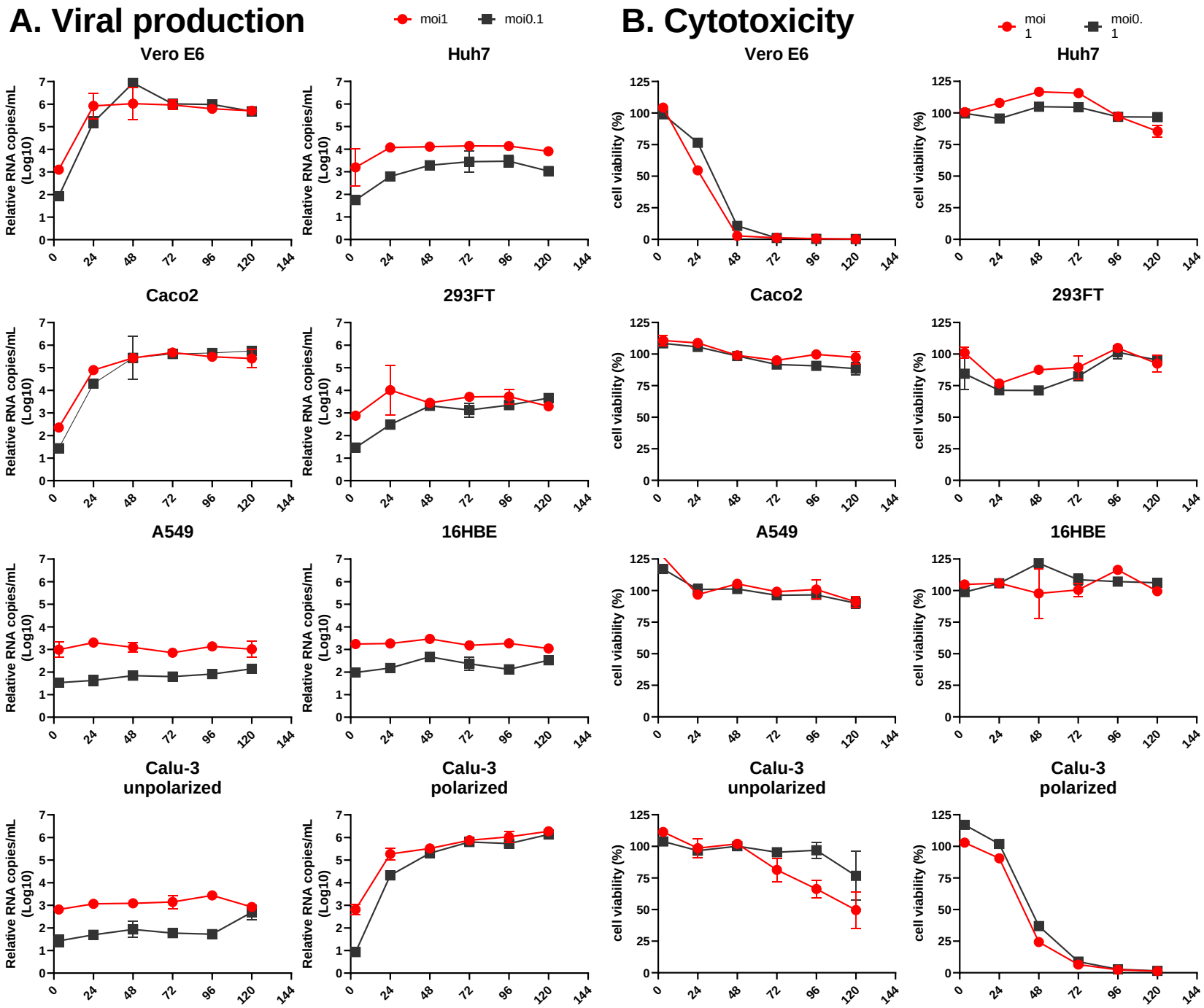
A. Viral production
moi1
moi0.1
B. Cytotoxicity
moi 1
moi0. 1
Vero E6
Huh7
Caco2
293FT
A549
16HBE
Calu-3 unpolarized
Calu-3 polarized
Relative RNA copies/mL (Log10)
cell viability (%)
0
24
48
72
96
120
144

Figure 2

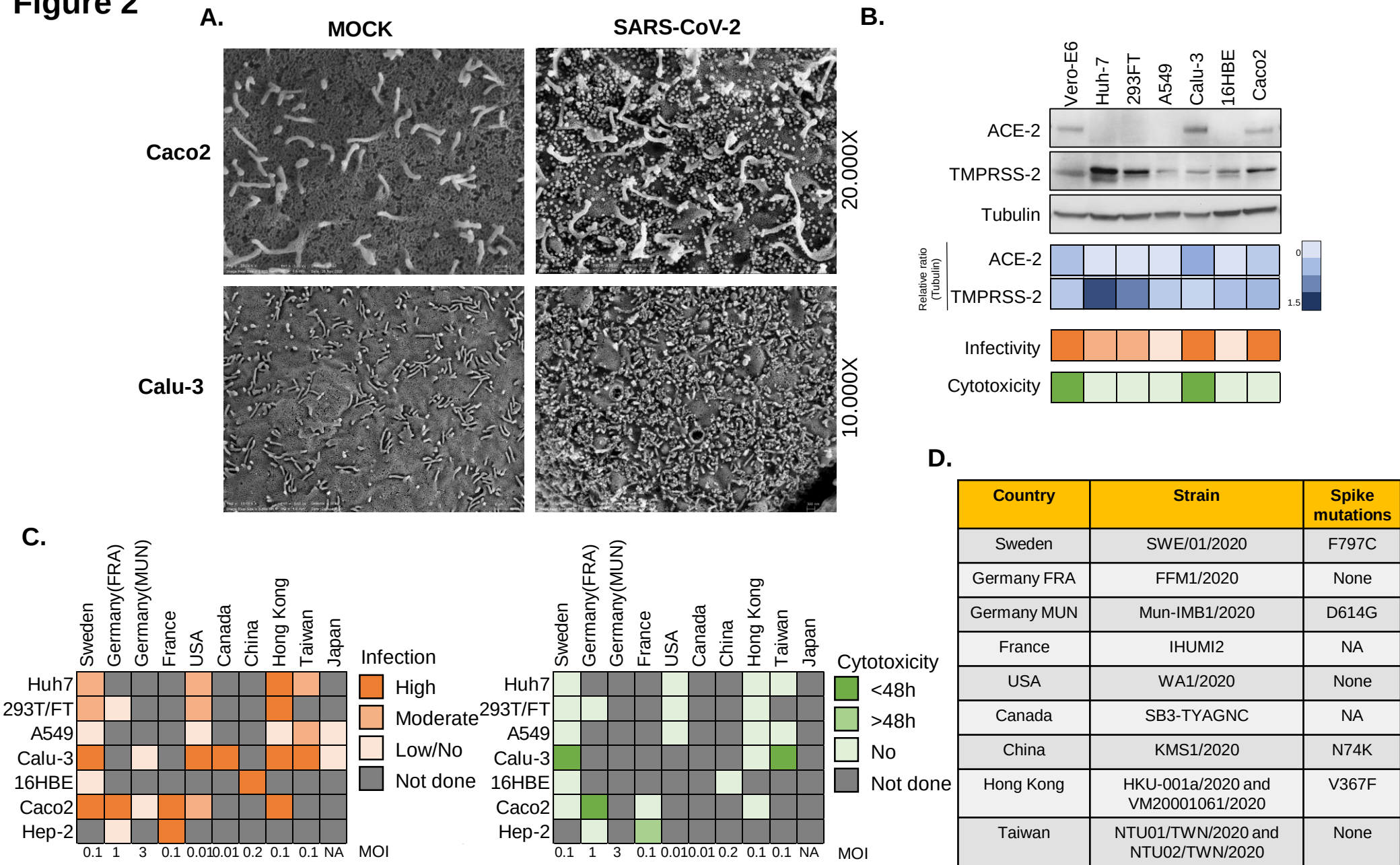

D.

Country	Strain	Spike mutations
Sweden	SWE/01/2020	F797C
Germany FRA	FFM1/2020	None
Germany MUN	Mun-IMB1/2020	D614G
France	IHUMI2	NA
USA	WA1/2020	None
Canada	SB3-TYAGNC	NA
China	KMS1/2020	N74K
Hong Kong	HKU-001a/2020 and VM20001061/2020	V367F
Taiwan	NTU01/TWN/2020 and NTU02/TWN/2020	None
Japan	TY-WK-521/2020	None

Figure 3

A.

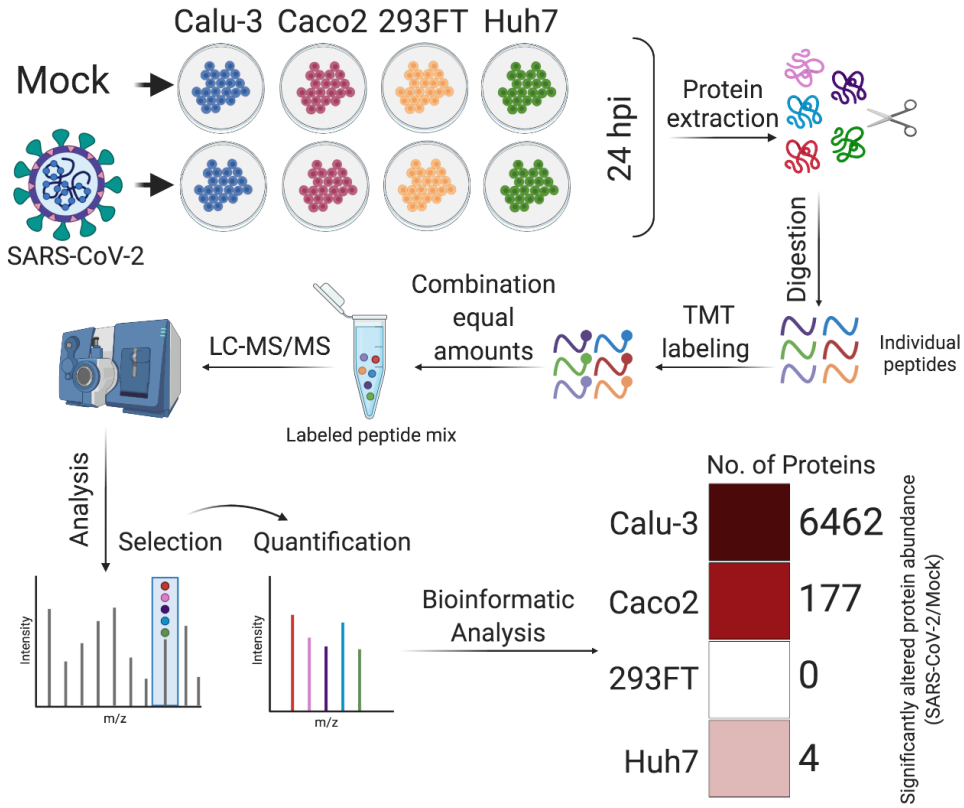
Calu-3 Caco2 293FT Huh7
Mock
SARS-CoV-2
24 hpi
Protein extraction
Digestion
Individual peptides
TMT labeling
Combination equal amounts
Labeled peptide mix
LC-MS/MS
Analysis
Selection
Quantification
Intensity
m/z
Bioinformatic Analysis
No. of Proteins
Calu-3 6462
Caco2 177
293FT 0
Huh7 4
Significantly altered protein abundance (SARS-CoV-2/Mock)

C.

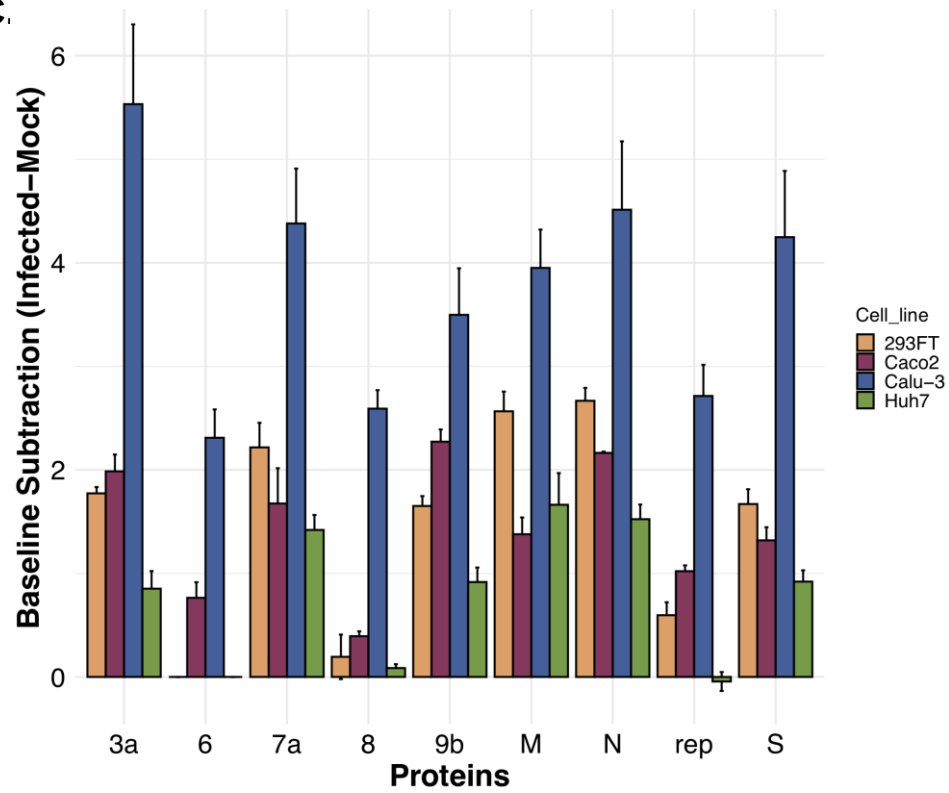
Baseline Subtraction (Infected−Mock)
0
2
4
6
3a
6
7a
8
9b
M
N
rep
S
Proteins
Cell_line
293FT
Caco2
Calu−3
Huh7

B.

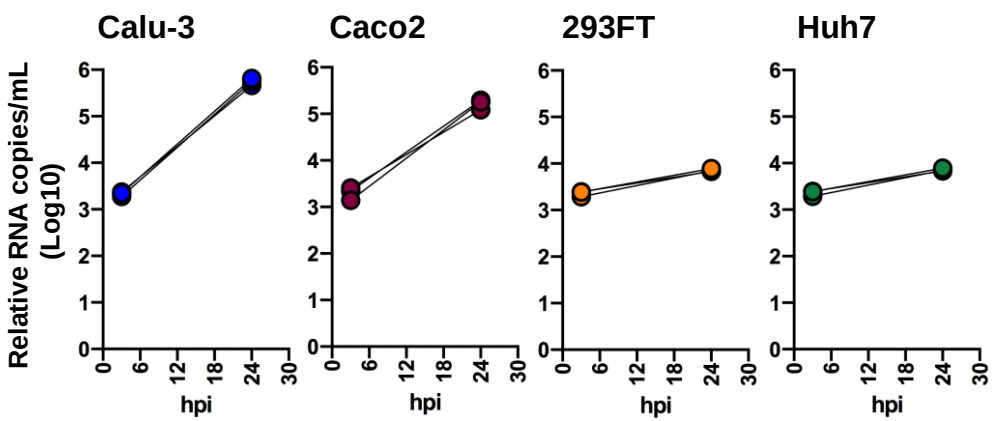
Calu-3
Caco2
293FT
Huh7
Relative RNA copies/mL (Log10)
0
1
2
3
4
5
6
0
6
12
18
24
30
hpi

Figure 4

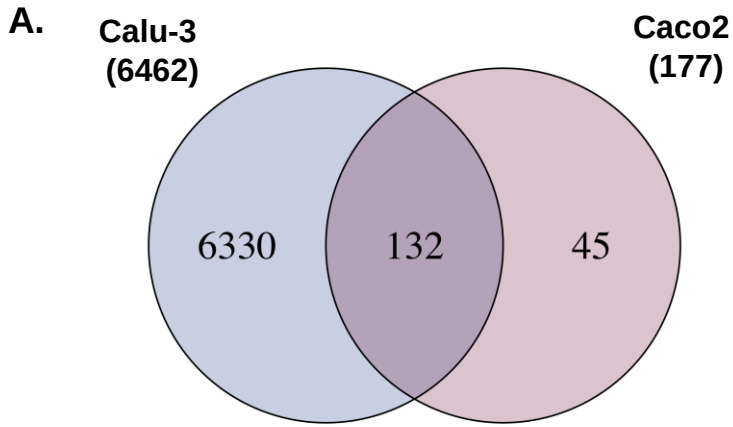
A.
Calu-3
(6462)
Caco2
(177)
6330
132
45

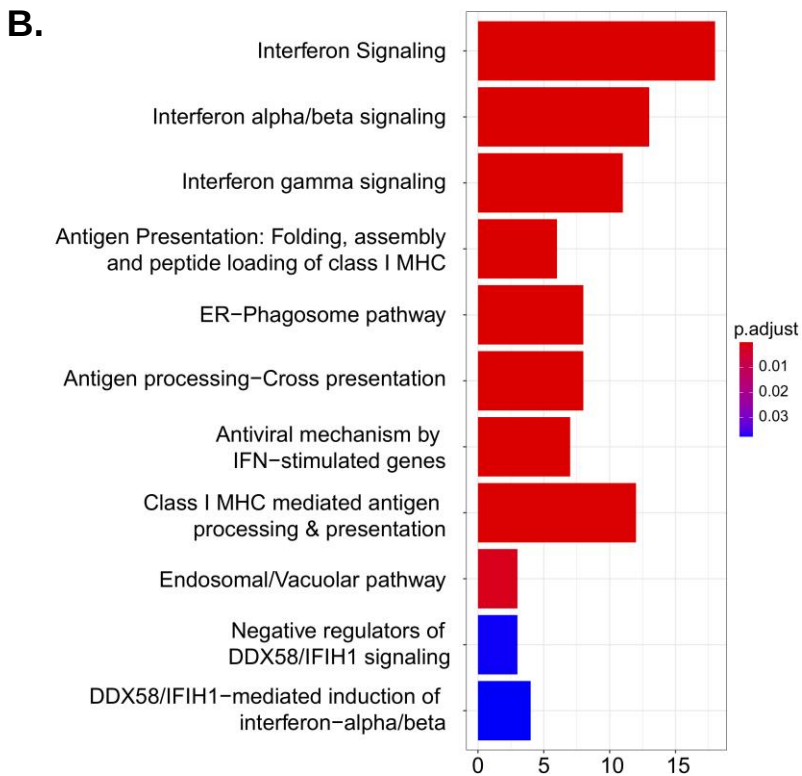
B.
Interferon Signaling
Interferon alpha/beta signaling
Interferon gamma signaling
Antigen Presentation: Folding, assembly and peptide loading of class I MHC
ER−Phagosome pathway
Antigen processing−Cross presentation
Antiviral mechanism by IFN−stimulated genes
Class I MHC mediated antigen processing & presentation
Endosomal/Vacuolar pathway
Negative regulators of DDX58/IFIH1 signaling
DDX58/IFIH1−mediated induction of interferon−alpha/beta
0
5
10
15
p.adjust
0.01
0.02
0.03

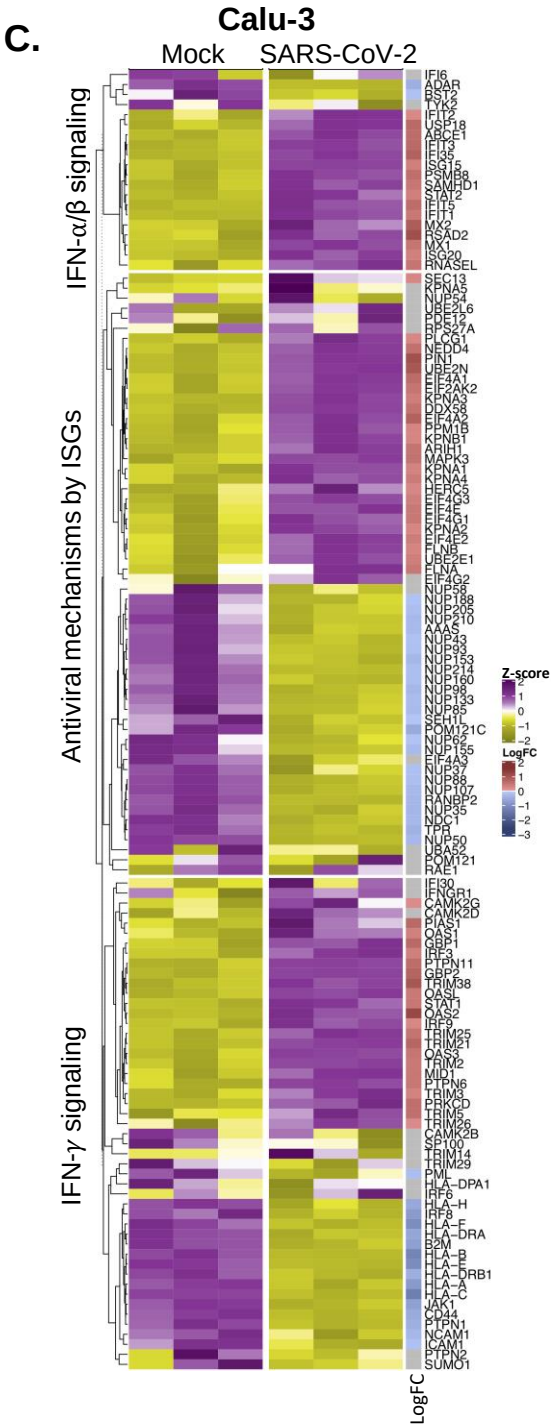
C.
Calu-3
Mock
SARS-CoV-2
IFN-α/β signaling
Antiviral mechanisms by ISGs
IFN-γ signaling
Z-score
LogFC

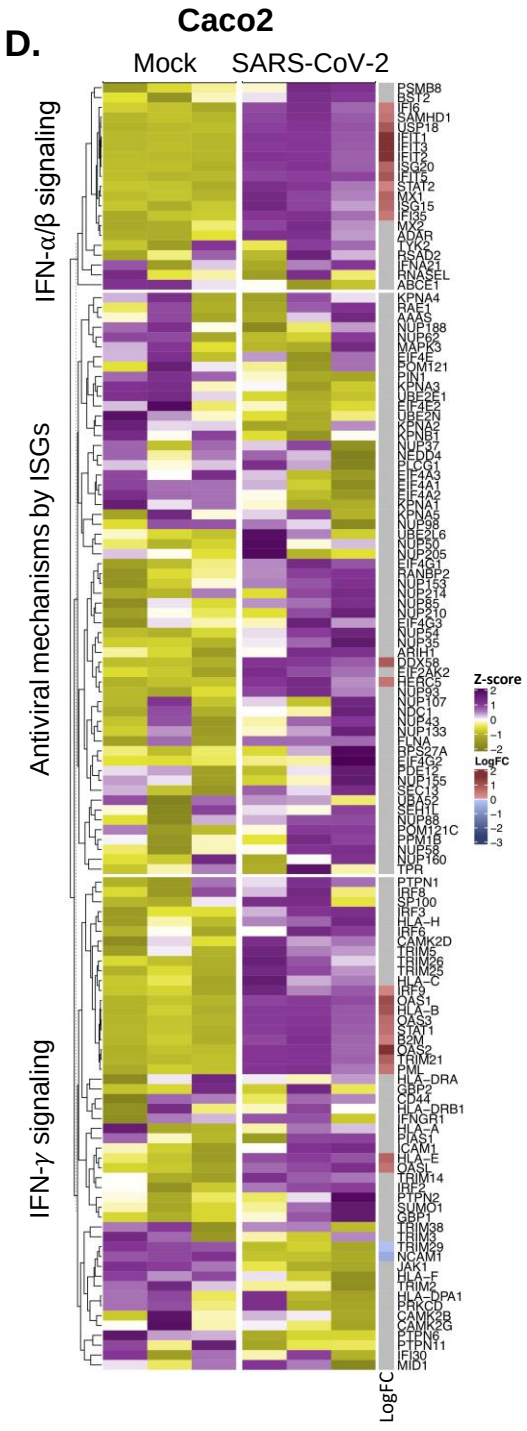
D.
Caco2
Mock
SARS-CoV-2
IFN-α/β signaling
Antiviral mechanisms by ISGs
IFN-γ signaling
Z-score
LogFC

Figure 5

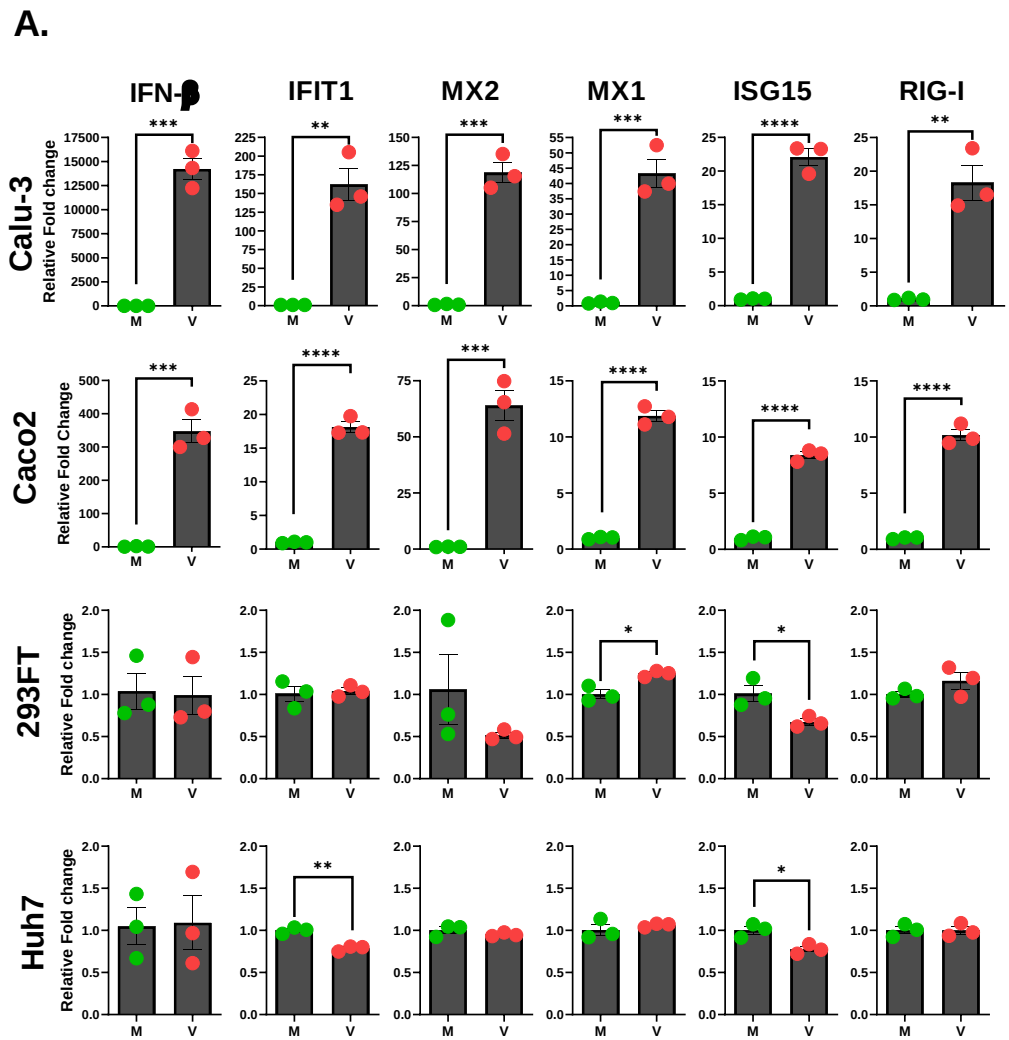
A.
IFN-β
IFIT1
MX2
MX1
ISG15
RIG-I
Calu-3
Caco2
293FT
Huh7
Relative Fold change
M
V

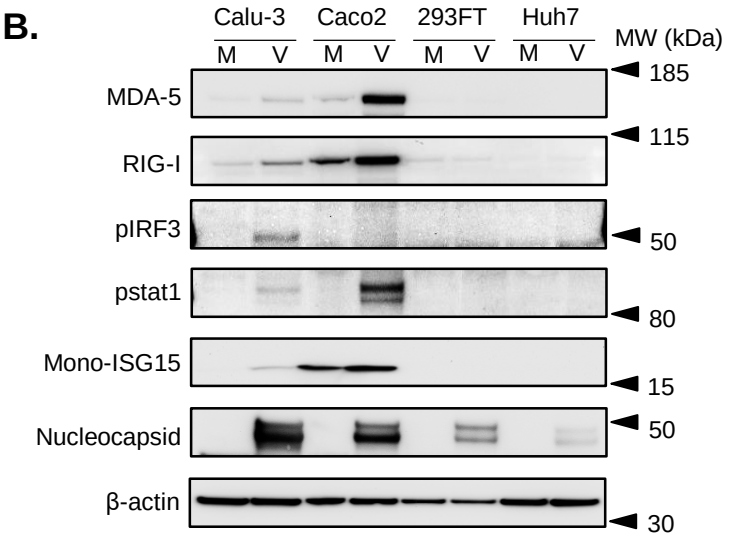
B.
Calu-3
Caco2
293FT
Huh7
M V M V M V M V
MW (kDa)
MDA-5
RIG-I
pIRF3
pstat1
Mono-ISG15
Nucleocapsid
β-actin
185
115
50
80
15
50
30

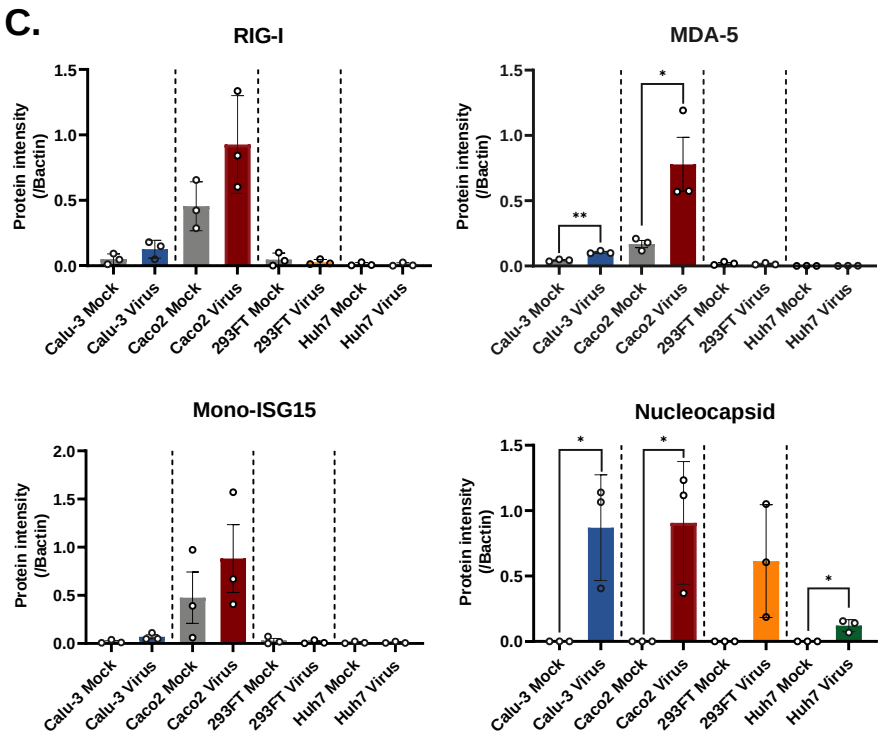
C.
RIG-I
MDA-5
Mono-ISG15
Nucleocapsid
Protein intensity (/Bactin)
Calu-3 Mock
Calu-3 Virus
Caco2 Mock
Caco2 Virus
293FT Mock
293FT Virus
Huh7 Mock
Huh7 Virus

Figure 6

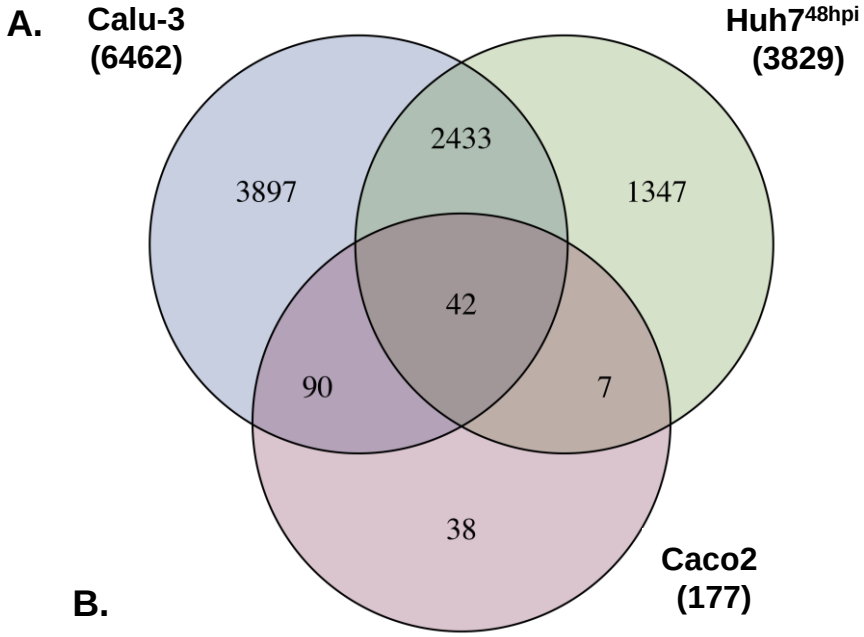
A.
Calu-3
(6462)
Huh7^48hpi
(3829)
Caco2
(177)
3897
2433
1347
42
90
7
38

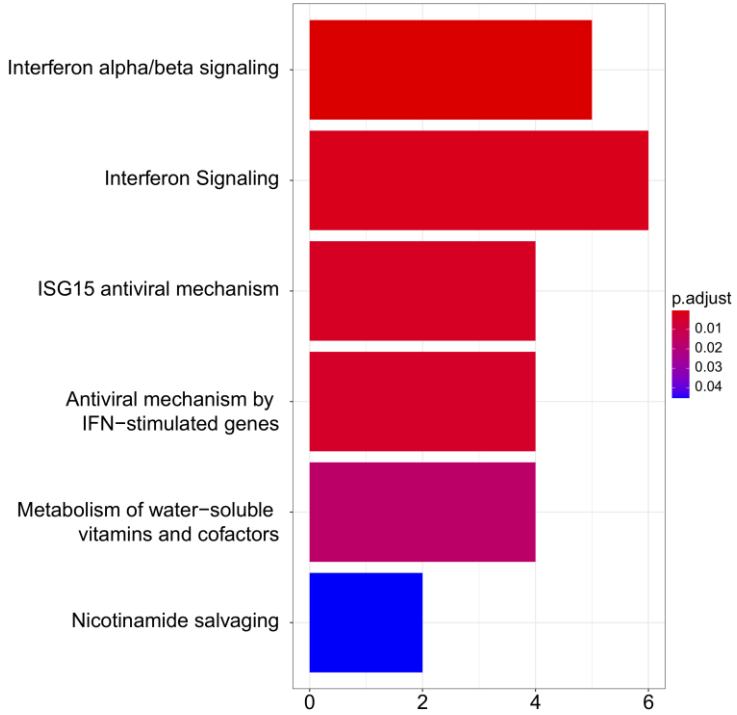
B.
Interferon alpha/beta signaling
Interferon Signaling
ISG15 antiviral mechanism
Antiviral mechanism by IFN−stimulated genes
Metabolism of water−soluble vitamins and cofactors
Nicotinamide salvaging
0
2
4
6
p.adjust
0.01
0.02
0.03
0.04

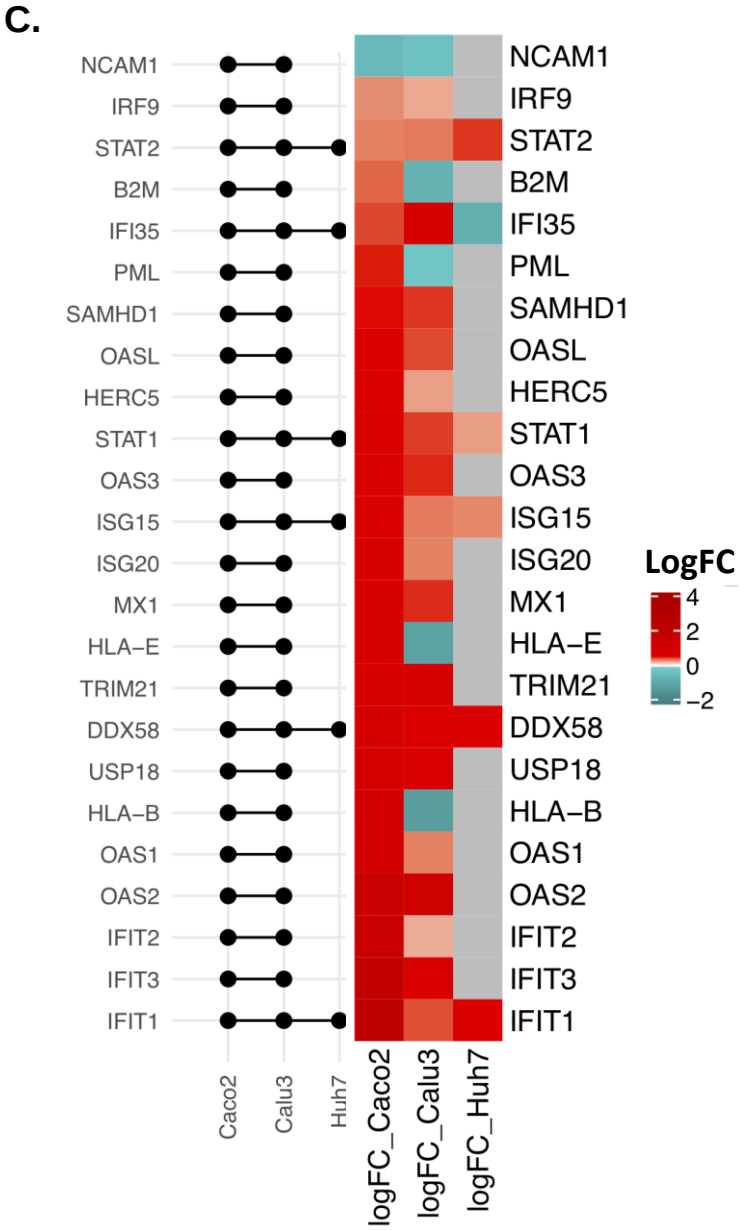
C.
NCAM1
IRF9
STAT2
B2M
IFI35
PML
SAMHD1
OASL
HERC5
STAT1
OAS3
ISG15
ISG20
MX1
HLA−E
TRIM21
DDX58
USP18
HLA−B
OAS1
OAS2
IFIT2
IFIT3
IFIT1
Caco2
Calu3
Huh7
logFC_Caco2
logFC_Calu3
logFC_Huh7
LogFC
4
2
0
−2

Figure 7

A.

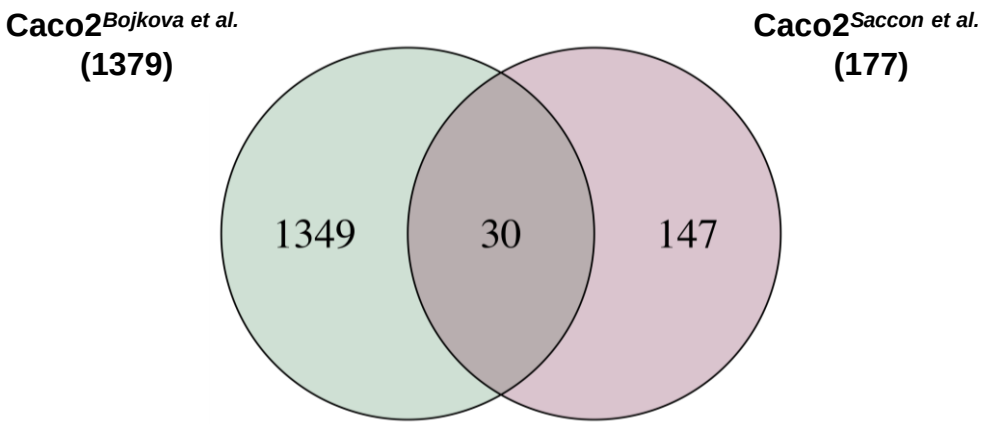
Caco2Bojkova et al.
(1379)
Caco2Saccon et al.
(177)
1349
30
147

B.

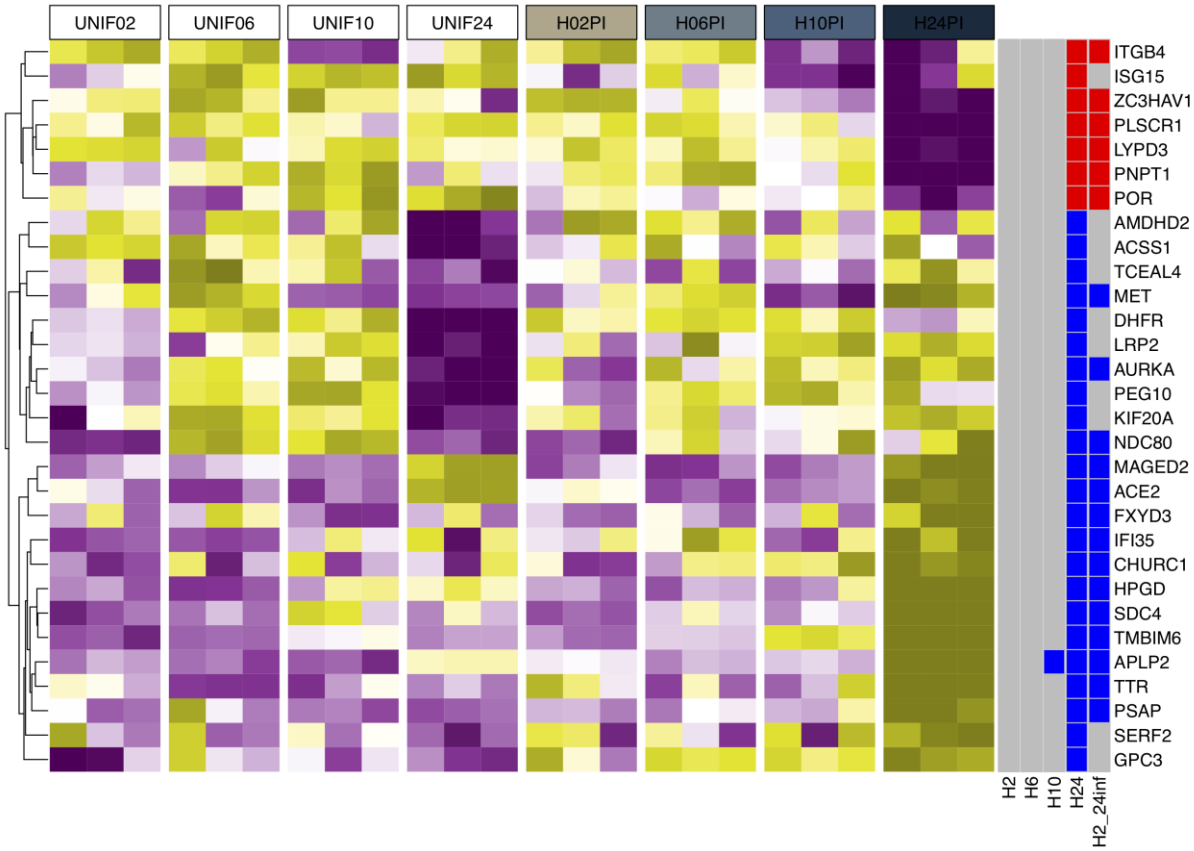
UNIF02
UNIF06
UNIF10
UNIF24
H02PI
H06PI
H10PI
H24PI
ITGB4
ISG15
ZC3HAV1
PLSCR1
LYPD3
PNPT1
POR
AMDHD2
ACSS1
TCEAL4
MET
DHFR
LRP2
AURKA
PEG10
KIF20A
NDC80
MAGED2
ACE2
FXYD3
IFI35
CHURC1
HPGD
SDC4
TMBIM6
APLP2
TTR
PSAP
SERF2
GPC3
H2
H6
H10
H24
H2_24inf

C.

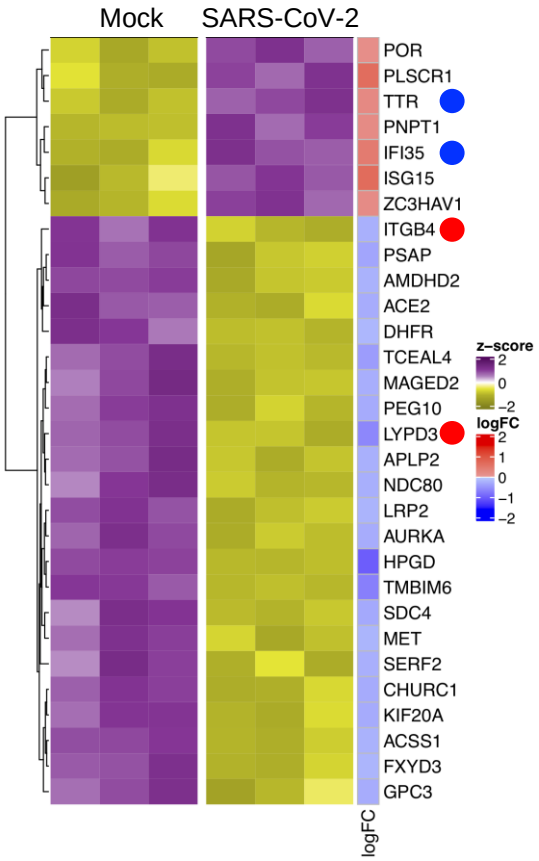
Mock
SARS-CoV-2
POR
PLSCR1
TTR
PNPT1
IFI35
ISG15
ZC3HAV1
ITGB4
PSAP
AMDHD2
ACE2
DHFR
TCEAL4
MAGED2
PEG10
LYPD3
APLP2
NDC80
LRP2
AURKA
HPGD
TMBIM6
SDC4
MET
SERF2
CHURC1
KIF20A
ACSS1
FXYD3
GPC3
logFC
z−score
2
0
−2
logFC
2
1
0
−1
−2